



Published in final edited form as:

Sci Transl Med. 2020 January 08; 12(525): . doi:10.1126/scitranslmed.aay5186.

Pancreatitis is an FGF21-deficient state that is corrected by replacement therapy

Genaro Hernandez¹, Ting Luo¹, Tanveer A. Javed², Li Wen³, Michael A. Kalwat¹, Kevin Vale¹, Farah Ammouri¹, Sohail Z. Husain⁴, Steven A. Kliewer^{1,5,*}, David J. Mangelsdorf^{1,6,*}

¹Department of Pharmacology, UT Southwestern Medical Center, Dallas, TX 75390, USA.

²Department of Pediatrics, University of Pittsburgh, Pittsburgh, PA 15224, USA.

³Department of Gastroenterology and Shanghai Key Laboratory of Pancreatic Disease, Shanghai General Hospital, Shanghai Jiao Tong University School of Medicine, Shanghai 200080, China.

⁴Department of Pediatrics, Stanford University, Palo Alto, CA 94305, USA.

⁵Department of Molecular Biology, UT Southwestern Medical Center, Dallas, TX 75390, USA.

⁶Howard Hughes Medical Institute, UT Southwestern Medical Center, Dallas, TX 75390, USA.

Abstract

The exocrine pancreas expresses the highest concentrations of fibroblast growth factor 21 (FGF21) in the body, where it maintains acinar cell proteostasis. Here, we showed in both mice and humans that acute and chronic pancreatitis is associated with a loss of FGF21 expression due to activation of the integrated stress response (ISR) pathway. Mechanistically, we found that activation of the ISR in cultured acinar cells and mouse pancreata induced the expression of ATF3, a transcriptional repressor that directly bound to specific sites on the *Fgf21* promoter and resulted in loss of FGF21 expression. These ATF3 binding sites are conserved in the human *FGF21* promoter. Consistent with the mouse studies, we also observed the reciprocal expression of ATF3 and FGF21 in the pancreata of human patients with pancreatitis. Using three different mouse models of pancreatitis, we showed that pharmacologic replacement of FGF21 mitigated the ISR and resolved pancreatitis. Likewise, inhibition of the ISR with an inhibitor of the PKR-like endoplasmic reticulum kinase (PERK) also restored FGF21 expression and alleviated pancreatitis. These findings highlight the importance of FGF21 in preserving exocrine pancreas function and suggest its therapeutic use for prevention and treatment of pancreatitis.

*Corresponding author. steven.kliewer@utsouthwestern.edu (S.A.K.); davo.mango@utsouthwestern.edu (D.J.M.).

Author contributions: G.H., S.Z.H., S.A.K., and D.J.M. designed the experiments and wrote the paper. G.H., T.L., T.A.J., L.W., M.A.K., F.A., and K.V. performed and analyzed experiments. S.Z.H., S.A.K., and D.J.M. supervised the project. All authors commented on and approved the paper.

Competing interests: The FGF21 protein was provided by Novo Nordisk. G.H., S.A.K., and D.J.M. collaborate with and have received travel reimbursement from Novo Nordisk and are authors on a patent related to this work ("Methods and compositions for the treatment of secretory disorders"; US20190201490A1 and WO2017205517A1).

Data and materials availability: All data related to this study can be found in the paper or Supplementary Materials. Mouse strains and plasmid DNA can be provided under a materials transfer agreement from UTSW.

INTRODUCTION

Pancreatitis is one of the most common and debilitating diseases of the gastrointestinal tract, leading to substantial morbidity and mortality (1). Pancreatitis results from the premature activation of digestive enzymes in the pancreas itself, which causes tissue damage and inflammation. Common causes of pancreatitis include alcohol abuse and gallstones (2). About a third of pancreatitis cases in humans are caused by alcohol, which has the highest rates of morbidity (2, 3). Pancreatitis also occurs in 5 to 10% of patients undergoing endoscopic retrograde cholangiopancreatography (ERCP), a procedure used to examine the pancreatic and biliary ducts as well as the gallbladder (2). Treatments for pancreatitis are limited and generally supportive in nature (2, 4–6). Thus, there is a pressing need for new therapies.

Fibroblast growth factor 21 (FGF21) is a hormone secreted by the liver in response to diverse metabolic stresses including starvation and the consumption of alcohol or simple sugars (7–9). FGF21 acts on a heteromeric cell surface receptor complex composed of a conventional FGF receptor, FGFR1c, together with an obligate co-receptor, β -klotho (7–9). FGF21 is also highly expressed in the exocrine pancreas, where it acts directly on acinar cells in an autocrine/paracrine manner to stimulate digestive enzyme secretion (10, 11). This prevents protein overload and relieves endoplasmic reticulum (ER) stress. Mice lacking FGF21 are particularly susceptible to pancreatitis induced by the cholecystokinin (CCK) analog cerulein (10, 12). Conversely, genetic overexpression of FGF21 confers protection in this model. Likewise, prophylactic FGF21 administration reduces fibrogenesis in a mouse model of L-arginine-induced chronic pancreatitis (13).

Here, we tested the hypothesis that loss of FGF21 is a principal driving factor of pancreatitis. On the basis of this concept, we further investigated using FGF21 therapeutically to reverse preexisting pancreatitis in cerulein- and alcohol-induced mouse models and to prevent pancreatitis in a murine model of ERCP.

RESULTS

FGF21 is down-regulated in pancreatitis

Pharmacologic FGF21 protects against cerulein-induced acute pancreatitis (CIP) (10, 12). To test whether endogenous FGF21 expression changes during CIP, we treated mice with seven hourly injections of cerulein and collected pancreas and blood samples at 4, 8, 12, and 18 hours after the first injection (fig. S1A). CIP was confirmed by histology (fig. S1B) and increased expression of genetic markers of inflammation (*Tnfa* and *Il6*) and oxidative (*Hmox1*) and ER stress (*Chop*) (fig. S1C). Consistent with previous observations (12), *Fgf21* mRNA was increased by CIP at the 4-hour time point but unchanged compared to vehicle at 8 hours (Fig. 1A). Unexpectedly, however, *Fgf21* expression markedly decreased at 12 hours and was virtually undetectable by 18 hours. Similarly, pancreatic FGF21 protein concentrations were elevated by CIP at 4 hours and then gradually decreased to undetectable by 18 hours (Fig. 1B). Plasma FGF21 concentrations remained low (<1.5 ng/ml) and were not affected by CIP (Fig. 1C). *Fgf21* expression was also suppressed in a chronic model of CIP (fig. S1, D and E), in which cerulein was injected on 6 days over the course of 2 weeks

(14, 15). Induction of CIP in this chronic model was confirmed by an increase in pancreatic myeloperoxidase (MPO) activity (fig. S1F) and genetic markers of inflammation (*Tnfa* and *Il6*) as well as oxidative stress (*Hmox1*) and ER stress (*Chop*) (fig. S1G).

To determine whether the loss of *Fgf21* is a general feature of pancreatitis, we investigated two other clinically relevant mouse models: alcohol-induced pancreatitis (AIP) and ERCP-induced pancreatitis (EIP) (14–19). AIP occurs within 24 hours after two injections of ethanol and its non-oxidative metabolite palmitoleic acid (POA) (fig. S1, H and I). Likewise, infusion of ERCP radiocontrast dye at high pressure into the pancreatic ducts of mice (fig. S1J) resulted in EIP (fig. S1K), similar to that observed in humans (2). As in CIP, AIP and EIP caused a marked decrease in pancreatic *Fgf21* (Fig. 1D). Thus, a hallmark feature of pancreatitis is the loss of pancreatic *Fgf21* expression.

Therapeutic administration of FGF21 reverses pancreatitis

To test whether therapeutic administration of FGF21 reverses pancreatitis, recombinant FGF21 was injected four times over a 12- to 16-hour period after induction of CIP (fig. S2A) and AIP (fig. S2B), and the mice were sacrificed 2 hours after the last FGF21 dose (fig. S2, A and B). FGF21 treatment increased plasma FGF21 concentrations to 10 to 15 ng/ml and restored pancreatic FGF21 protein (but not mRNA) expression in both CIP (Fig. 1E) and AIP (Fig. 1F). FGF21 treatment reversed all of the sequelae of pancreatitis in both the CIP and AIP models, which included restoring plasma amylase (Fig. 1, G and H) and pancreatic MPO (Fig. 1, I and J) activities to normal and markedly reducing pancreatic edema, inflammatory infiltrate, necrosis, and the combined overall severity score of these parameters (Fig. 1, K and L, and fig. S2, C and D). FGF21 treatment also reduced pancreatic gene expression markers of inflammation and oxidative and ER stress (fig. S2, E and F). Thus, therapeutic administration of FGF21 rescues the loss of endogenous FGF21 in the pancreas and thereby decreases injury due to pancreatitis. Although plasma FGF21 concentrations were induced in the AIP model (Fig. 1F), which was expected on the basis of ethanol's ability to induce hepatic *Fgf21* expression (20), this did not restore FGF21 concentrations in the pancreas and was insufficient to reverse pancreatitis.

We also explored FGF21's potential to prevent EIP by mixing FGF21 in with the radiocontrast agent and thereby locally administering FGF21 directly into the exocrine pancreas during the ductal infusion procedure (fig. S2G). Intraductal administration of FGF21, which restricts the recombinant FGF21 to the pancreas and its duct, maintained normal endogenous pancreatic FGF21 mRNA and protein expression without increasing plasma FGF21 concentrations (Fig. 1M). FGF21 treatment by this method also strongly protected against EIP-induced changes in serum amylase (Fig. 1N) and pancreatic MPO activity (Fig. 1O) as well as pancreatic histology and gene expression (Fig. 1P and fig. S2, H and I). These results indicate that FGF21 is efficacious therapeutically to both treat and prevent various causes of pancreatitis.

FGF21 reverses pancreatitis by acting directly on the exocrine pancreas

Endogenous FGF21 acts in an autocrine/paracrine manner on pancreatic acinar cells to induce digestive enzyme secretion and maintain proteostasis (10). To test whether

recombinant FGF21 acts directly on pancreatic acinar cells to elicit its therapeutic effects, we used *Klb^{Cela1}* mice, in which *Klb* expression was selectively disrupted in acinar cells using a tamoxifen-inducible elastase-Cre driver (10). We confirmed the reduction in *Klb* expression after tamoxifen administration by quantitative polymerase chain reaction (qPCR) (Fig. 2A). Basal pancreatic FGF21 mRNA (Fig. 2B), but not protein (Fig. 2C), was lower in *Klb^{Cela1}* than in control *Klb^{fl/fl}* mice. CIP repressed FGF21 mRNA (Fig. 2B) and protein (Fig. 2C) expression in both *Klb^{Cela1}* and *Klb^{fl/fl}* mice. Administration of exogenous FGF21 increased plasma FGF21 markedly (Fig. 2D), restored FGF21 protein concentrations to normal in pancreas (Fig. 2C), lowered plasma amylase activity (Fig. 2E), and reduced pancreatic edema, inflammatory infiltrate, and necrosis caused by CIP in *Klb^{fl/fl}*, but not in *Klb^{Cela1}*, mice (Fig. 2, F and G). FGF21 administration also reversed CIP-mediated induction of gene markers of inflammation and ER and oxidative stress in *Klb^{fl/fl}*, but not in *Klb^{Cela1}*, mice (Fig. 2H). We conclude that FGF21 acts directly on the acinar cells of the exocrine pancreas to mediate its therapeutic effects.

ATF3 represses FGF21 expression in pancreatitis

The transcription factor ATF4, which is induced by the PKR-like endoplasmic reticulum kinase (PERK) arm of the integrated stress response (ISR), is a strong inducer of FGF21 expression in the liver and muscle (21–24). Mice lacking the related transcription factor ATF3 have elevated pancreatic *Fgf21* mRNA in response to cerulein treatment (25). Because ATF3 is induced by ATF4 and can repress its activity, we examined the roles of these two transcription factors in regulating pancreatic FGF21 in the context of CIP. Pancreatic ATF4 mRNA (fig. S3A) and protein (Fig. 3, A and B) concentrations were induced 4 hours into CIP but returned to basal between 8 and 18 hours (Fig. 3, A and B, and fig. S3A). In contrast, ATF3 mRNA (fig. S3B) and protein (Fig. 3, A and C) expression, which are absent under normal physiological conditions, were markedly elevated at all time points after cerulein treatment. We also examined pancreatic *Atf3* and *Atf4* expression in the chronic CIP (fig. S3C), AIP (fig. S3D), and EIP (fig. S3E) models. *Atf3* mRNA was elevated in all models, whereas *Atf4* was decreased in chronic CIP and unchanged in AIP and EIP (fig. S3, C to E). Thus, ATF3 and ATF4 were differentially regulated in all four models of pancreatitis.

As part of these time course studies, we also analyzed ATF3 and ATF4 occupancy on the *Fgf21* promoter by chromatin immunoprecipitation (ChIP)–qPCR. The *Fgf21* promoter contains three ATF4 response elements (AAREs) (Fig. 3D). All three AAREs are conserved in the mouse and human *FGF21* promoter (21, 26). We analyzed the AARE1 and AARE3 sites together (AARE1 + 3), because they are only 10 base pairs (bp) apart (Fig. 3D). ATF4 binding to the AARE1 + 3 sites increased at 4 hours after induction of CIP but decreased at 12 and 18 hours compared to the saline-treated control mice (Fig. 3E). ATF3 binding to the AARE1 + 3 site also increased at 4 hours of CIP but, unlike ATF4, was maintained throughout the experiment (Fig. 3F). We detected little or no ATF4 (Fig. 3G and fig. S3F) or ATF3 (Fig. 3H and fig. S3G) on the AARE2 or control sites. These data suggest that CIP-mediated induction of ATF3 suppresses *Fgf21* transcription by competing with ATF4 for binding to the *Fgf21* promoter.

We further examined the contribution of ATF3 to CIP-mediated repression of *Fgf21* using the 266–6 mouse acinar cell line. Treatment of cells with cerulein recapitulated the repression of *Fgf21* mRNA observed in vivo (Fig. 4A). In cell-based reporter assays, an *Fgf21* promoter construct that included all three amino acid response elements was repressed by cerulein (Fig. 4B). Knockdown of ATF3 by small interfering RNA (siRNA) (fig. S4A) increased basal *Fgf21* promoter activity and blocked its repression by cerulein (Fig. 4B). Conversely, ATF3 overexpression repressed the *Fgf21* promoter (Fig. 4C). Overexpressing ATF4 increased reporter activity, whereas overexpressing ATF3 reduced it (Fig. 4D). Titrating ATF3 against a fixed amount of ATF4 (fig. S4, B to D) caused a dose-dependent repression of *Fgf21* promoter activity, reaching full repression at an ATF3-to-ATF4 ratio of about 100:1 (Fig. 4E). This ratio is consistent with that observed in vivo due to pancreatitis (Fig. 3, A to C). Together, these data show that ATF3 represses *Fgf21* gene expression. Promoter loss-of-function mutations in each of the individual AAREs (Fig. 4D) and promoter truncation mutants (Fig. 4F) revealed that AARE1 is the principal site for induction and repression by ATF4 and ATF3, respectively. Accordingly, cerulein failed to repress *Fgf21* promoter activity in the AARE1 mutant (Fig. 4G). Thus, ATF3 and ATF4 control *Fgf21* expression primarily by competing for the AARE1 element.

Dysregulation of the ATF4/ATF3/FGF21 axis is conserved in human pancreatitis

We explored the translational relevance of our findings by analyzing pancreata from chronic and acute pancreatitis patients (data file S1). As expected, there was a high degree of fibrosis, edema, and inflammation in sections from patients with pancreatitis (Fig. 5A). Consistent with our mouse studies, ATF3 expression was increased (Fig. 5, B and C), and FGF21 (Fig. 5, D and E) and ATF4 (Fig. 5, F and G) expression was decreased in patients with chronic and acute pancreatitis. These findings indicate that human pancreatitis is associated with a loss of FGF21 that correlates with an increased ATF3:ATF4 ratio.

PERK inhibition reverses pancreatitis in an FGF21-dependent manner

A prediction of our findings is that PERK inhibition would block pancreatitis-mediated induction of ATF3 in the pancreas, thereby providing another tractable target for therapeutic intervention. Accordingly, mice administered the PERK inhibitor GSK2656157 were refractory to CIP-mediated repression of FGF21 mRNA and protein (Fig. 6, A and B). Therapeutic administration of GSK2656157 also lowered plasma amylase activity to near normal (Fig. 6C) and improved pancreatic histology (Fig. 6, D and E) and mRNA markers of inflammation and oxidative and ER stress (Fig. 6F). The protective effects of GSK2656157 were completely absent in FGF21-KO (knockout) mice (Fig. 6, C to F), further supporting the idea that the loss of FGF21 is a major contributor to pancreatitis. Moreover, the finding that PERK inhibition reverses pancreatitis by restoring endogenous FGF21 expression reinforces the notion that FGF21 replacement therapy may be an effective way to treat pancreatitis.

DISCUSSION

Here, we have examined the utility of using FGF21 therapeutically to treat pancreatitis. We show that FGF21 in the pancreas is markedly reduced in human pancreatitis as well as

MATERIALS AND METHODS

Study design

This study was designed to characterize the effect of pancreatitis on the FGF21 pathway by analyzing the samples of pancreata from mice and humans with acute and chronic forms of the disease. On the basis of the finding that pancreatitis was universally associated with a loss of FGF21, we then investigated the efficacy of FGF21 replacement therapy in three murine models of pancreatitis that mimic the acute and chronic disease observed in humans. Accordingly, the endpoints for the in vivo experiments assessed FGF21 concentrations in pancreas and plasma and pancreatitis severity. Cell culture experiments were designed to characterize the molecular mechanism underlying FGF21 down-regulation by pancreatitis. Measurements of plasma/serum amylase and pancreatic MPO activities, histological grading, and gene expression markers were used to assess the degree of pancreatitis. All histological grading was performed in a blinded fashion with the samples de-identified before submission for grading. For all in vivo experiments, mice were age- and weight-matched across experimental groups. Sample size (n) is defined as biological replicates for in vivo experiments and technical replicates (N) for cell culture experiments. Sample size for human pancreatitis tissue was determined by availability. For all in vivo experiments, sample sizes of $n = 3$ to 8 mice per group were used, and for cell culture experiments, $n = 4$ to 8 were used to achieve 20% differences between treatment groups or genotype-dependent effects at 80% power with a 95% confidence interval ($\alpha = 0.05$). In vivo experiments were performed twice ($n = 2$) and cell culture experiments were performed three times ($n = 3$) to verify their reproducibility. Outliers were identified using the ROUT method (GraphPad Prism).

Recombinant FGF21

Recombinant human FGF21 used in all the experiments was a gift from Novo Nordisk.

Quantitative real-time PCR

RNA from pancreas or cells was extracted using RNA Stat-60 (Iso-Tex Diagnostics). Complementary DNA (cDNA) was generated from RNA (2 μ g) using the High-Capacity cDNA Reverse Transcription Kit (Life Technologies). qPCR was performed by the SYBR Green method (29). Primer sequences for the genes analyzed can be found in table S1. *U36B4* (NM_007475) was used as the reference mRNA.

Mice

The Institutional Animal Care and Research Advisory Committee of the University of Texas Southwestern Medical Center and the University of Pittsburgh School of Medicine approved all experiments. Mice were housed in a pathogen-free facility and fed a standard chow diet (Harlan Teklad). C57BL/6J mice were purchased through the University of Texas Southwestern Mouse Breeding Core. Swiss Webster mice were purchased from Charles River Laboratories. FGF21-KO (*Fgf21^{tm1.2Djm}*) (30) inducible acinar cell-specific β -klotho KO mice (*Klb^{Cela1}*) (10) and wild-type littermates were maintained on a C57BL/6J background. Male mice were used for all experiments, except for the EIP studies, where

female Swiss Webster mice were used. In *Klb^{Cela1}* mice, Cre expression was induced via intraperitoneal injection of tamoxifen (50 µg/g) (Sigma) for three consecutive days, followed by *Klb* KO validation by qPCR for experiments 2 weeks later.

CIP and FGF21 treatment

Acute pancreatitis was induced by administration of seven hourly intraperitoneal injections of cerulein (50 µg/kg) (Tocris Bioscience), whereas mice in the control group were injected with saline. For the therapeutic treatments, FGF21 (1 mg/kg) and GSK2656157 (25 mg/kg) (Cayman Chemical) were administered intraperitoneally four times after CIP. In studies where GSK2656157 was used, the vehicle injected was 5% dimethyl sulfoxide (DMSO) diluted in saline to facilitate the solubilization of GSK2656157.

Chronic pancreatitis

To induce chronic CIP, C57BL/6J mice were given six hourly intraperitoneal injections of cerulein (50 µg/kg; Tocris Bioscience) per day for 6 days during the course of 2 weeks.

AIP and FGF21 treatment

Male Swiss Webster mice were given ethanol (1.3 g/kg) in combination with POA (150 mg/kg) twice intraperitoneally over 1 hour to induce AIP. FGF21 was administered four times intraperitoneally at 1 mg/kg before collecting tissue and plasma, 24 hours after the induction of AIP.

EIP and FGF21 treatment

ERCP was performed as previously described (17–19). Female Swiss Webster mice were used for these experiments, which were performed at the University of Pittsburgh. Iohexol (300 mg/ml) (Omnipaque 300, GE Healthcare) was the radiocontrast agent infused intraductally. Where indicated, FGF21 was combined with the radiocontrast agent at a final concentration of 1 µg/ml. Plasma was collected at 6 and 24 hours. Tissues were harvested 24 hours after ERCP.

Amylase and pancreatic MPO activity

Amylase activity in mouse plasma/serum was measured using an amylase assay kit (Abcam). MPO activity was measured from pancreas homogenized in MPO assay buffer using an MPO activity assay kit (Sigma).

Histology

Mouse pancreas was harvested and fixed in 10% neutral buffered formalin overnight at 4°C. Paraffin sections were embedded, sectioned, and hematoxylin and eosin (H&E)-stained by the UT Southwestern (UTSW) Molecular Pathology Core. Paraffin-embedded pancreas sections were deparaffinized in xylene and rehydrated through an ethanol gradient (100, 95, 70, and 50%). Antigen retrieval was performed for 30 min in citric acid-based antigen unmasking solution (Vector Laboratories) before immunofluorescence. H&E-stained pancreas was graded on an equal weight score (from 0 to 3) for edema (0 = absent; 1 = focally increased between lobules; 2 = diffusely increased; 3 = acini disrupted and

separated), inflammatory infiltration (0 = absent; 1 = in ducts, around ductal margins; 2 = in the parenchyma, <50% of the lobules; 3 = in the parenchyma, >50% of the lobules), necrosis (0 = absent; 1 = periductal necrosis, <5% of cells; 2 = focal necrosis, 5 to 20% of cells; 3 = diffuse parenchymal necrosis, 20 to 50% of cells), and total severity score (sum of edema, inflammatory infiltrate, and necrosis scores) as previously described (31). Five different fields per mouse pancreas were analyzed in a blinded fashion. Images were acquired with a Zeiss Axio Scan.Z1 slide scanner.

Immunofluorescence

Sections were incubated for 1 hour in blocking buffer [1% bovine serum albumin (BSA), 5% normal donkey serum, and 0.3% Triton X-100 in 1× phosphate-buffered saline (PBS)], followed by overnight incubation at 4°C with primary antibodies in blocking buffer (table S2). Sections were washed in 1× PBS three times for 5 min each time, followed by incubation for 1 hour with Alexa Fluor–conjugated secondary antibodies against the primary antibody’s host species in blocking buffer. Sections were washed in 1× PBS three times for 5 min each time, stained with 4',6-diamidino-2-phenylindole (DAPI) (Life Technologies), and mounted with Aqua-Poly/Mount (Polysciences).

Immunoblotting

Pancreas was homogenized using FastPrep-24 lysing matrix bead tubes (MP Biomedicals), and cells were homogenized by passaging through an insulin syringe in 1× radioimmunoprecipitation assay buffer (Cell Signaling Technology) supplemented with a cocktail of protease and phosphatase inhibitors (Roche). Protein lysate concentrations were measured using the DC Protein Assay (Bio-Rad). Equal protein amounts were loaded and electrophoresed in a 4 to 20% SDS–polyacrylamide gel electrophoresis gel (Bio-Rad) and transferred to nitrocellulose membranes (Bio-Rad). Membranes were blocked with 5% BSA in tris-buffered saline with 0.5% Tween 20 for 1 hour. Probing of membranes with primary antibodies was performed overnight at 4°C (table S2). Membranes were then incubated with horseradish peroxidase–conjugated secondary antibodies (Cell Signaling Technology) against the primary antibody’s host species for 1 hour. Membranes were developed using the Clarity ECL substrate solution (Bio-Rad), and the signal was detected with an ImageQuant LAS 4000 luminescent imager (General Electric). Quantification was done using ImageJ.

Chromatin immunoprecipitation

ChIP assays were performed using the SimpleChIP Plus Enzymatic Chromatin IP Kit with magnetic beads (Cell Signaling Technology). Twenty-five milligrams from each mouse pancreas was used for each immunoprecipitation, and 4% of the total isolated digested chromatin was used as input. Primer sequences for the sites analyzed by qPCR are in table S3.

Enzyme-linked immunosorbent assay

Mouse FGF21 in either plasma or pancreatic tissue was measured using a mouse FGF21 enzyme-linked immunosorbent assay (ELISA) kit (BioVendor).

Plasmids

The full-length mouse *Fgf21* promoter (−1497/+5) firefly luciferase reporter construct and its truncated versions were generated as previously described (32). For AARE mutagenesis experiments, the full-length *Fgf21* promoter reporter construct was mutated, as shown in Fig. 3D. Mouse ATF3 and ATF4 expression plasmids were purchased from GenScript. Empty expression vector [pcDNA3.1+/C-(K)DYK] was used as a control. The *Renilla* luciferase pRL-CMV reporter vector was used as the normalizing control in the dual-luciferase reporter assays (Promega). Mouse ATF3 siRNA was purchased as a pool of three to four targeting siRNAs (Santa Cruz Biotechnology).

Cell culture and transfection assays

266–6 cells were cultured in 10% fetal bovine serum in Dulbecco's modified Eagle's medium (DMEM) (Life Technologies) with antibiotics. Cells were transfected by incubating either plasmids or siRNA with Lipofectamine 2000 (Life Technologies) for 6 hours in serum and antibiotic-free DMEM in a 96-well plate. At 6 hours, the transfection medium was replaced with complete medium and the cells were incubated for another 18 hours. Cells were treated with vehicle, 100 nM cerulein, or 100 nM GSK2656157 for another 12 hours before measuring luciferase activity. Where indicated, 100 ng of *Fgf21* promoter-luciferase or truncated versions was transfected per well. One nanogram of *Atf3* or *Atf4* expression plasmid and pRL-CMV (*Renilla* luciferase control) were cotransfected per well. The pcDNA3.1+/C-(K)DYK empty vector was used to bring the final amount of DNA to 200 ng per well. In the ATF3 dose response experiment, the ATF3 and pcDNA3.1+/C-(K)DYK amounts were modulated to reach the appropriate ATF3 dosing. Where indicated, 5 pmol of ATF3 siRNA was transfected. Cells were washed once in 1× PBS and lysed in 1× passive lysis buffer (Promega) and incubated for 15 min on an orbital shaker for 15 min before measuring luciferase activities with a dual-luciferase assay kit (Promega).

Human pancreatic tissue samples

Pancreas samples from 14 healthy individuals and 52 individuals with pancreatitis were procured via the University of Texas Southwestern Tissue Resource, a shared resource at the Simmons Comprehensive Cancer Center (UTSW CC), the National Disease Research Interchange (NDRI), and US Biomax (tissue arrays PA804a and BBS14011). The pancreas biopsies from patients were paraffin- embedded, sectioned, and H&E-stained by the UTSW CC. Pancreatitis was confirmed from the histological samples by the pathologist at the University of Texas Southwestern Tissue Resource. Tissue immunofluorescence for FGF21, ATF3, and ATF4 was performed as described above for paraffin-embedded sections. Clinical data corresponding to the samples analyzed and obtained either through the UTSW CC, NDRI, or US Biomax were de-identified and are available in data file S1. The samples from NDRI were procured and processed under protocol DKAM14 to M.A.K.

Statistical analyses

Nonparametric, two-tailed Student's *t* test was used for two-group analyses. One-way and two-way analyses of variance (ANOVAs) with Newman-Keuls post hoc correction (GraphPad Prism) were used for multiple group analyses. Data are presented as the mean ±

SEM; $P < 0.05$ was considered significant. Raw data from this study are available in data file S2.

Supplementary Material

Refer to Web version on PubMed Central for supplementary material.

Acknowledgments

We thank B. Andersen (Novo Nordisk) for providing recombinant FGF21 and Y. Zhang and M. Grzemska for their support with the mouse experiments.

Funding: This work was supported by the NIH (grants R01DK067158 and P01AG051459 to S.A.K. and D.J.M.; grants R01DK093491 and R01DK103002 to S.Z.H.), the Robert A. Welch Foundation (grants I-1558 to S.A.K. and I-1275 to D.J.M.), a Ford Foundation Fellowship (to G.H.), the Juvenile Diabetes Research Foundation (SRA-2019-702-Q-R to M.A.K.), the UTSW NCI Cancer Center (grant 5P30CA142543 to S.A.K. and D.J.M.), and the Howard Hughes Medical Institute (to D.J.M.).

REFERENCES AND NOTES

1. Peery AF, Crockett SD, Murphy CC, Lund JL, Dellon ES, Williams JL, Jensen ET, Shaheen NJ, Barritt AS, Lieber SR, Kochar B, Barnes EL, Fan YC, Pate V, Galanko J, Baron TH, Sandler RS, Burden and cost of gastrointestinal, liver, and pancreatic diseases in the United States: Update 2018. *Gastroenterology* 156, 254–272.e11 (2019). [PubMed: 30315778]
2. Conwell DL, Banks PA, Greenberger NJ, in Harrison's Principles of Internal Medicine, 20e, Jameson JL, Fauci AS, Kasper DL, Hauser SL, Longo DL, Loscalzo J, Eds. (McGraw-Hill Education, 2018).
3. Chowdhury P, Gupta P, Pathophysiology of alcoholic pancreatitis: An overview. *World J. Gastroenterol* 12, 7421–7427 (2006). [PubMed: 17167828]
4. Arvanitakis M, Dumonceau JM, Albert J, Badaoui A, Bali MA, Barthet M, Besselink M, Deviere J, Oliveira Ferreira A, Gyokeres T, Hritz I, Hucl T, Milashka M, Papanikolaou IS, Poley JW, Seewald S, Vanbiervliet G, van Lienden K, van Santvoort H, Voermans R, Delhaye M, van Hooft J, Endoscopic management of acute necrotizing pancreatitis: European Society of Gastrointestinal Endoscopy (ESGE) evidence-based multidisciplinary guidelines. *Endoscopy* 50, 524–546 (2018). [PubMed: 29631305]
5. Forsmark CE, Andersen DK, Farrar JT, Golden M, Habtezion A, Husain SZ, Li L, Mayerle J, Pandol SJ, Uc A, Zhu Z, Yadav D, Accelerating the drug delivery pipeline for acute and chronic pancreatitis: Summary of the working group on drug development and trials in chronic pancreatitis at the national institute of diabetes and digestive and kidney diseases workshop. *Pancreas* 47, 1200–1207 (2018). [PubMed: 30325858]
6. Tenner S, Baillie J, DeWitt J, Vege SS; American College of Gastroenterology, American College of Gastroenterology guideline: Management of acute pancreatitis. *Am. J. Gastroenterol* 108, 1400–1415; 1416 (2013). [PubMed: 23896955]
7. BonDurant LD, Potthoff MJ, Fibroblast growth factor 21: A versatile regulator of metabolic homeostasis. *Annu. Rev. Nutr* 38, 173–196 (2018). [PubMed: 29727594]
8. Fisher FM, Maratos-Flier E, Understanding the physiology of FGF21. *Annu. Rev. Physiol* 78, 223–241 (2016). [PubMed: 26654352]
9. Kliewer SA, Mangelsdorf DJ, A dozen years of discovery: Insights into the Physiology and Pharmacology of FGF21. *Cell Metab.* 29, 246–253 (2019). [PubMed: 30726758]
10. Coate KC, Hernandez G, Thorne CA, Sun S, Le TDV, Vale K, Kliewer SA, Mangelsdorf DJ, FGF21 is an exocrine pancreas secretagogue. *Cell Metab.* 25, 472–480 (2017). [PubMed: 28089565]
11. Fon Tacer K, Bookout AL, Ding X, Kurosu H, John GB, Wang L, Goetz R, Mohammadi M, Kuro-o M, Mangelsdorf DJ, Kliewer SA, Research resource: Comprehensive expression atlas of the

- fibroblast growth factor system in adult mouse. *Mol. Endocrinol* 24, 2050–2064 (2010). [PubMed: 20667984]
12. Johnson CL, Weston JY, Chadi SA, Fazio EN, Huff MW, Kharitonov A, Koester A, Pin CL, Fibroblast growth factor 21 reduces the severity of cerulein-induced pancreatitis in mice. *Gastroenterology* 137, 1795–1804 (2009). [PubMed: 19664632]
 13. Wang N, Zhao T.-t., Li S.-m., Li Y.-h., Wang Y.-j., Li D.-s., Wang W.-f., Fibroblast growth factor 21 ameliorates pancreatic fibrogenesis via regulating polarization of macrophages. *Exp. Cell Res* 382, 111457 (2019). [PubMed: 31175853]
 14. Bansod S, Khurana A, Godugu C, Cerulein-induced chronic pancreatitis in Swiss albino mice: An improved short-term model for pharmacological screening. *J. Pharmacol. Toxicol. Methods* 96, 46–55 (2019). [PubMed: 30684670]
 15. Ulmasov B, Oshima K, Rodriguez MG, Cox RD, Neuschwander-Tetri BA, Differences in the degree of cerulein-induced chronic pancreatitis in C57BL/6 mouse substrains lead to new insights in identification of potential risk factors in the development of chronic pancreatitis. *Am. J. Pathol* 183, 692–708 (2013). [PubMed: 23845568]
 16. Huang W, Booth DM, Cane MC, Chvanov M, Javed MA, Elliott VL, Armstrong JA, Dingsdale H, Cash N, Li Y, Greenhalf W, Mukherjee R, Kaphalia BS, Jaffar M, Petersen OH, Tepikin AV, Sutton R, Criddle DN, Fatty acid ethyl ester synthase inhibition ameliorates ethanol-induced Ca²⁺-dependent mitochondrial dysfunction and acute pancreatitis. *Gut* 63, 1313–1324 (2014). [PubMed: 24162590]
 17. Jin S, Orabi AI, Le T, Javed TA, Sah S, Eisses JF, Bottino R, Molkentin JD, Husain SZ, Exposure to radiocontrast agents induces pancreatic inflammation by activation of nuclear factor- κ B, calcium signaling, and calcineurin. *Gastroenterology* 149, 753–764 (2015). [PubMed: 25980752]
 18. Orabi AI, Wen L, Javed TA, Le T, Guo P, Sanker S, Ricks D, Boggs K, Eisses JF, Castro C, Xiao X, Prasad K, Esni F, Gittes GK, Husain SZ, Targeted inhibition of pancreatic acinar cell calcineurin is a novel strategy to prevent post-ERCP pancreatitis. *Cell. Mol. Gastroenterol. Hepatol* 3, 119–128 (2017). [PubMed: 28090570]
 19. Wen L, Javed TA, Yimlamai D, Mukherjee A, Xiao X, Husain SZ, Transient high pressure in pancreatic ducts promotes inflammation and alters tight junctions via calcineurin signaling in mice. *Gastroenterology* 155, 1250–1263.e5 (2018). [PubMed: 29928898]
 20. Zhao C, Liu Y, Xiao J, Liu L, Chen S, Mohammadi M, McClain CJ, Li X, Feng W, FGF21 mediates alcohol-induced adipose tissue lipolysis by activation of systemic release of catecholamine in mice. *J. Lipid Res* 56, 1481–1491 (2015). [PubMed: 26092866]
 21. De Sousa-Coelho AL, Marrero PF, Haro D, Activating transcription factor 4-dependent induction of FGF21 during amino acid deprivation. *Biochem. J* 443, 165–171 (2012). [PubMed: 22233381]
 22. Kim KH, Jeong YT, Oh H, Kim SH, Cho JM, Kim Y-N, Kim SS, Kim DH, Hur KY, Kim HK, Ko T, Han J, Kim HL, Kim J, Back SH, Komatsu M, Chen H, Chan DC, Konishi M, Itoh N, Choi CS, Lee MS, Autophagy deficiency leads to protection from obesity and insulin resistance by inducing Fgf21 as a mitokine. *Nat. Med* 19, 83–92 (2013). [PubMed: 23202295]
 23. Wan XS, Lu XH, Xiao YC, Lin Y, Zhu H, Ding T, Yang Y, Huang Y, Zhang Y, Liu YL, Xu ZM, Xiao J, Li XK, ATF4- and CHOP-dependent induction of FGF21 through endoplasmic reticulum stress. *Biomed. Res. Int* 2014, 807874 (2014). [PubMed: 24900988]
 24. Shimizu N, Maruyama T, Yoshikawa N, Matsumiya R, Ma Y, Ito N, Tasaka Y, Kuribara-Souta A, Miyata K, Oike Y, Berger S, Schutz G, Takeda S, Tanaka H, A muscle-liver-fat signalling axis is essential for central control of adaptive adipose remodelling. *Nat. Commun* 6, 6693 (2015). [PubMed: 25827749]
 25. Fazio EN, Young CC, Toma J, Levy M, Berger KR, Johnson CL, Mehmood R, Swan P, Chu A, Cregan SP, Dilworth FJ, Howlett CJ, Pin CL, Activating transcription factor 3 promotes loss of the acinar cell phenotype in response to cerulein-induced pancreatitis in mice. *Mol. Biol. Cell* 28, 2347–2359 (2017). [PubMed: 28701342]
 26. Maruyama R, Shimizu M, Li J, Inoue J, Sato R, Fibroblast growth factor 21 induction by activating transcription factor 4 is regulated through three amino acid response elements in its promoter region. *Biosci. Biotechnol. Biochem* 80, 929–934 (2016). [PubMed: 27010621]

27. Johnson CL, Mehmood R, Laing SW, Stepniak CV, Kharitonov A, Pin CL, Silencing of the fibroblast growth factor 21 gene is an underlying cause of acinar cell injury in mice lacking MIST1. *Am. J. Physiol. Endocrinol. Metab* 306, E916–E928 (2014). [PubMed: 24549397]
28. Waldron RT, Pandol S, Lugea A, Groblewski G, Endoplasmic reticulum stress and the unfolded protein response in exocrine pancreas physiology and pancreatitis (Pancreapedia: Exocrine Pancreas Knowledge Base, 2015).
29. Bookout AL, Cummins CL, Mangelsdorf DJ, Pesola JM, Kramer MF, High-throughput real-time quantitative reverse transcription PCR. *Curr. Protoc. Mol. Biol* 73, 15.8.1–15.8.28 (2006).
30. Potthoff MJ, Inagaki T, Satapati S, Ding X, He T, Goetz R, Mohammadi M, Finck BN, Mangelsdorf DJ, Kliewer SA, Burgess SC, FGF21 induces PGC-1alpha and regulates carbohydrate and fatty acid metabolism during the adaptive starvation response. *Proc. Natl. Acad. Sci. U.S.A* 106, 10853–10858 (2009). [PubMed: 19541642]
31. Wildi S, Kleeff J, Mayerle J, Zimmermann A, Bottinger EP, Wakefield L, Buchler MW, Friess H, Korc M, Suppression of transforming growth factor beta signalling aborts caerulein induced pancreatitis and eliminates restricted stimulation at high caerulein concentrations. *Gut* 56, 685–692 (2007). [PubMed: 17135311]
32. Inagaki T, Dutchak P, Zhao G, Ding X, Gautron L, Parameswara V, Li Y, Goetz R, Mohammadi M, Esser V, Elmquist JK, Gerard RD, Burgess SC, Hammer RE, Mangelsdorf DJ, Kliewer SA, Endocrine regulation of the fasting response by PPARalpha-mediated induction of fibroblast growth factor 21. *Cell Metab.* 5, 415–425 (2007). [PubMed: 17550777]

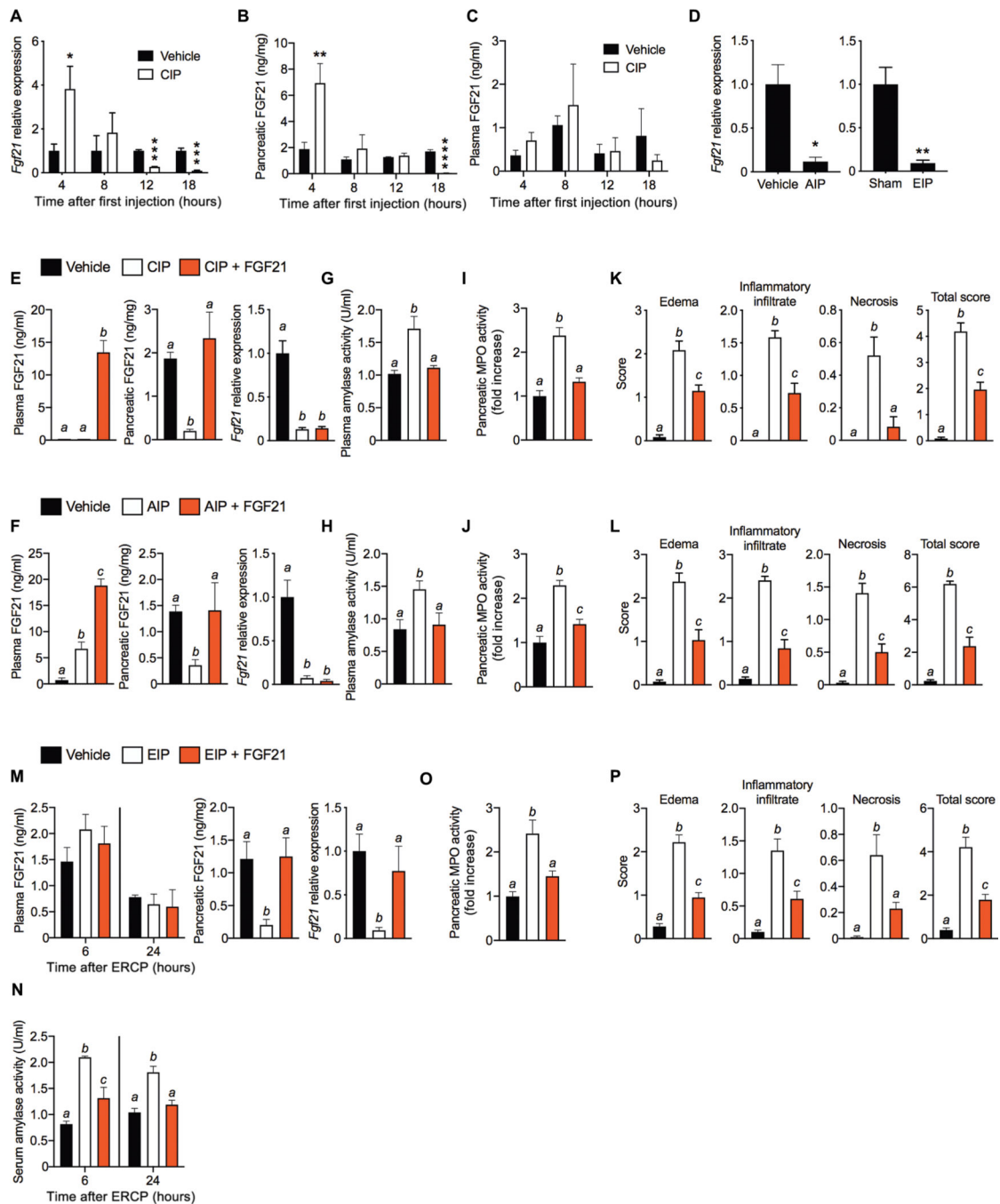


Fig. 1. FGF21 replacement ameliorates pancreatitis.

(A to C) Pancreatic FGF21 mRNA (A) and protein (B), and plasma FGF21 (C) at 4, 8, 12, or 18 hours after the first cerulein injection in CIP. (D) Pancreatic *Fgf21* mRNA after 24 hours of AIP and EIP. (E and F) Pancreatic FGF21 mRNA and protein and plasma FGF21 protein in CIP (E) or AIP (F) after a 24-hour treatment regimen of FGF21 (1 mg/kg) (four intraperitoneal injections). (G and H) Plasma amylase activity in CIP (G) and AIP (H). (I and J). Pancreatic MPO activity in CIP (I) and AIP (J). (K and L) Histological grading of mouse pancreata in CIP (K) and AIP (L). (M) FGF21 in plasma (at 6 and 24 hours), and

pancreatic FGF21 mRNA and protein (at 24 hours) after inducing EIP with intraductal infusion of contrast agent in the absence or presence of FGF21 (100 µg/ml). (N) Serum amylase activity at 6 and 24 hours from mice in (M). (O and P) Pancreatic MPO activity (O) and histological grading of pancreata (P) of mice in (M). Results are expressed as means ± SEM. *n* = number of mice per group for all experiments. *n* = 3 to 4 in (A) to (C); *n* = 3 for AIP and *n* = 5 for EIP in (D); *n* = 6 in (E), (G), (I), and (K); *n* = 8 in (F), (H), (J), and (L); *n* = 5 in (M) to (P). **P* < 0.05; ***P* < 0.01; ****P* < 0.001; *****P* < 0.0001. Asterisks indicate statistically different values relative to vehicle. Statistical differences (*P* > 0.05) are indicated between all values that have different letters.

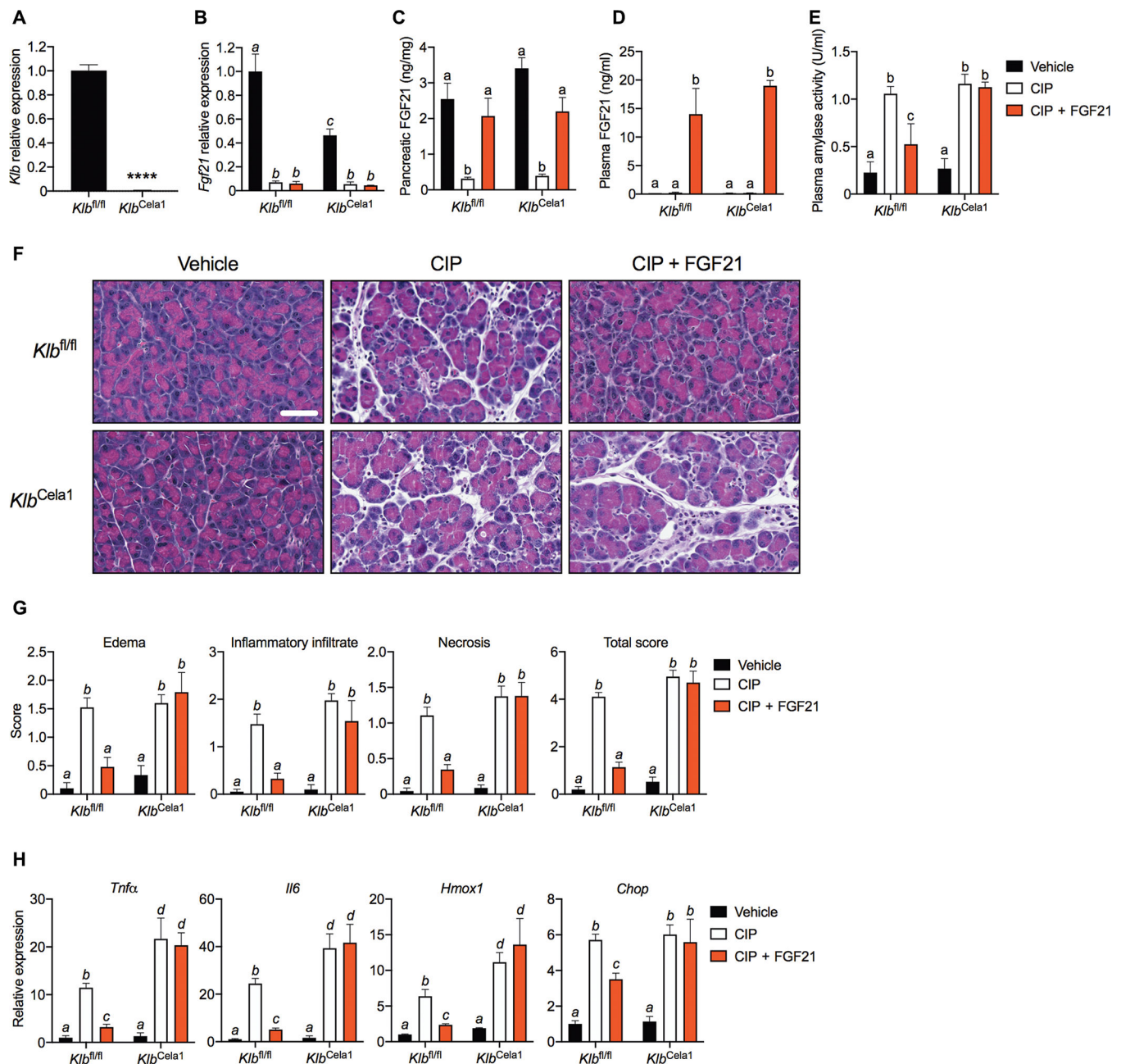


Fig. 2. β-Klotho in acinar cells is required for the therapeutic effects of FGF21 in pancreatitis.

(A) Pancreatic *Klb* mRNA in wild-type (*Klb^{fl/fl}*) and acinar cell-specific β-klotho KO (*Klb^{Cela1}*) mice ($n = 3$). (B and C) Pancreatic FGF21 mRNA (B) and protein (C) in CIP after a 24-hour treatment regimen of FGF21 (1 mg/kg) (four intraperitoneal injections) in *Klb^{fl/fl}* and *Klb^{Cela1}* mice. (D and E) Plasma FGF21 (D) and amylase activity (E) of mice in (B). (F and G) Representative H&E images of stained pancreata (F) and histological grading (G) of mice in (B). Scale bar indicates 50 μm for all images. (H) Pancreatic inflammation (*Tnfα* and *Il6*), oxidative stress (*Hmox1*), and ER stress (*Chop*) markers of mice in (B). Results are expressed as means ± SEM. n , number of mice per group. $n = 3$ (vehicle), 4 (CIP), and 5 (CIP + FGF21) in (B) to (G). **** $P < 0.0001$. Asterisks indicate statistically different values

relative to vehicle. Statistical differences ($P > 0.05$) are indicated between all values that have different letters.

Author Manuscript

Author Manuscript

Author Manuscript

Author Manuscript

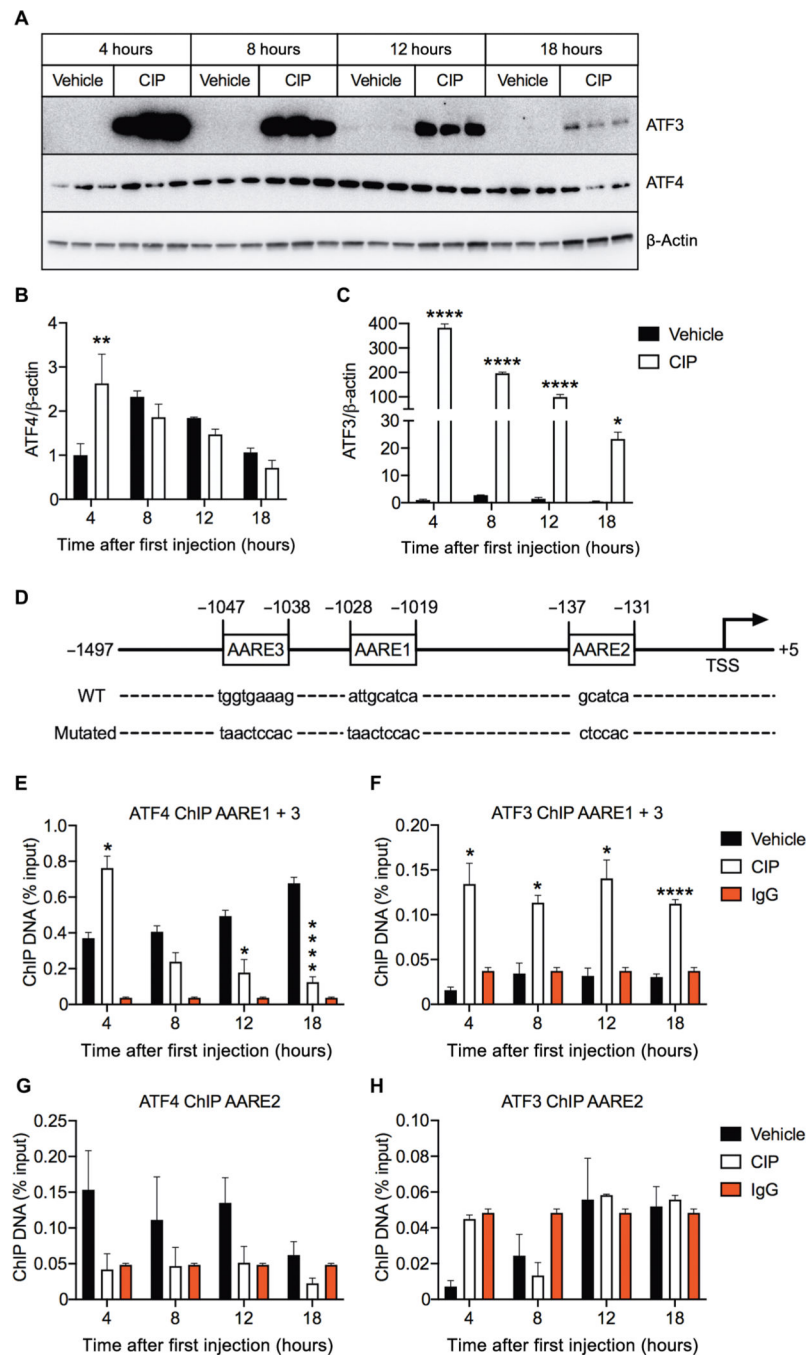


Fig. 3. ATF3 is induced in pancreatitis and binds to the *Fgf21* promoter.

(A) Immunoblot of pancreatic ATF4 and ATF3 at 4, 8, 12, or 18 hours after the first cerulein injection in CIP with β -actin as loading control. (B and C) Quantification of ATF4 (B) and ATF3 (C) in (A). (D) Schematic of the mouse $-1497/+5$ bp region of the *Fgf21* promoter with the sequences and positions of the wild-type (WT) and mutant amino acid response elements (AARE). (E to H) ChIP assays quantified by qPCR for ATF4 (E and G) and ATF3 (F and H) binding to the AARE1 + 3 or AARE2 response elements from mouse pancreas in the CIP time-course experiment. IgG, immunoglobulin G. Results are expressed as means \pm

SEM. $n = 3$ to 4 mice per group for all experiments. $*P < 0.05$; $**P < 0.01$; $****P < 0.0001$. Asterisks indicate statistically different values relative to vehicle.

Author Manuscript

Author Manuscript

Author Manuscript

Author Manuscript

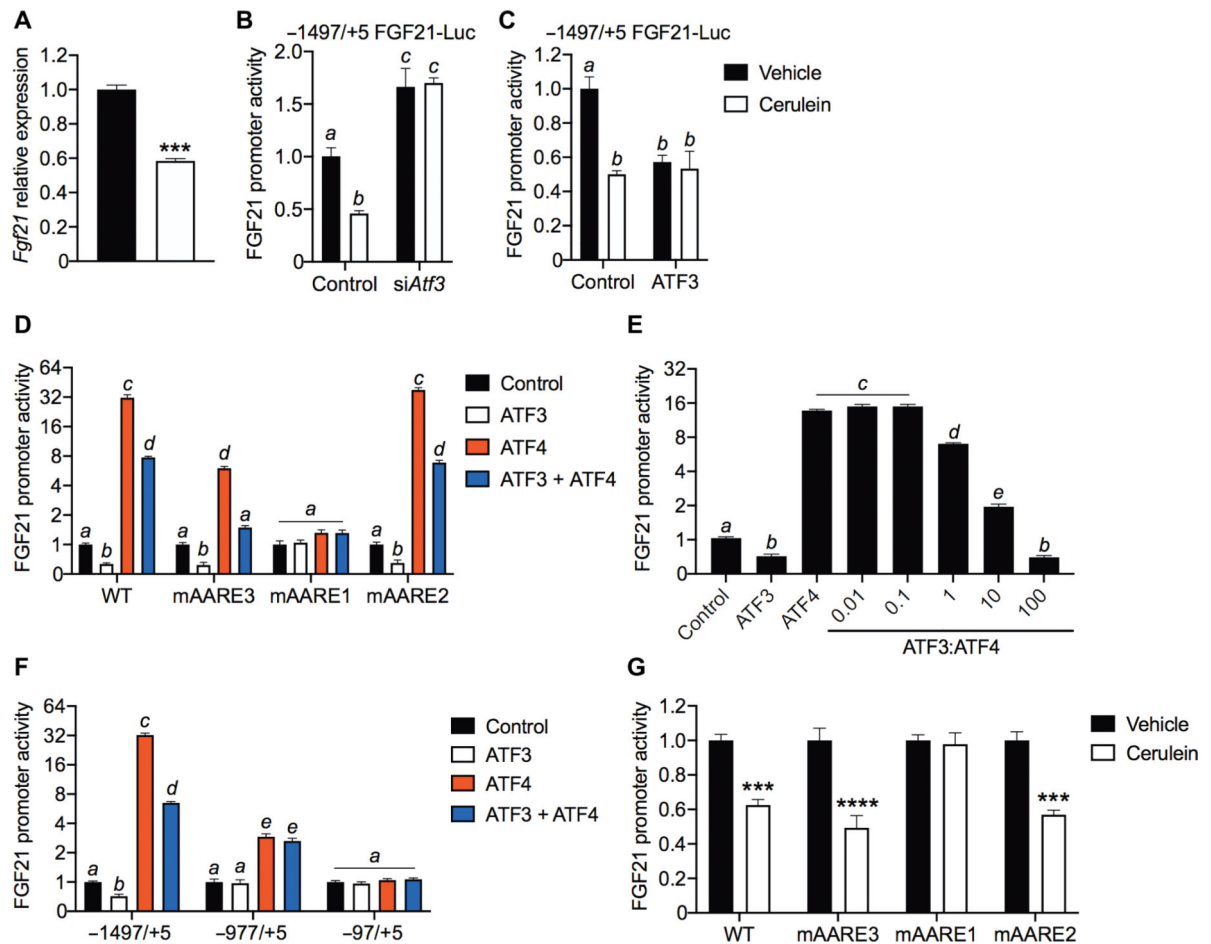


Fig. 4. ATF3 competes with ATF4 to repress *Fgf21* promoter activity.

(A) *Fgf21* mRNA in 266-6 mouse acinar cells treated with vehicle (black bar) or 100 nM cerulein (white bar) for 12 hours ($N=3$). (B and C) Repression of the *Fgf21* promoter using a luciferase reporter gene evaluated after *Atf3* siRNA knockdown ($N=4$) (B) or ATF3 overexpression ($N=4$) (C) in 266-6 cells treated as in (A). (D) Wild-type and AARE mutant *Fgf21* promoter luciferase (Luc) activity in 266-6 cells overexpressing ATF3 and ATF4 ($N=4$). (E) *Fgf21* promoter luciferase activity in 266-6 cells expressing increasing amounts (0.01 to 100 ng) of ATF3 expression plasmid and a fixed amount (1 ng) of ATF4 expression plasmid ($N=8$). (F) Truncated *Fgf21* promoter luciferase assays in 266-6 cells overexpressing ATF3 and ATF4 ($N=6$). (G) Wild-type and AARE mutant *Fgf21* promoter luciferase activity in 266-6 cells treated as in (A) ($N=4$). Results are expressed as means \pm SEM. N , number of replicates. *** $P < 0.001$; **** $P < 0.0001$. Asterisks indicate statistically different values relative to vehicle. Statistical differences ($P > 0.05$) are indicated between all values that have different letters.

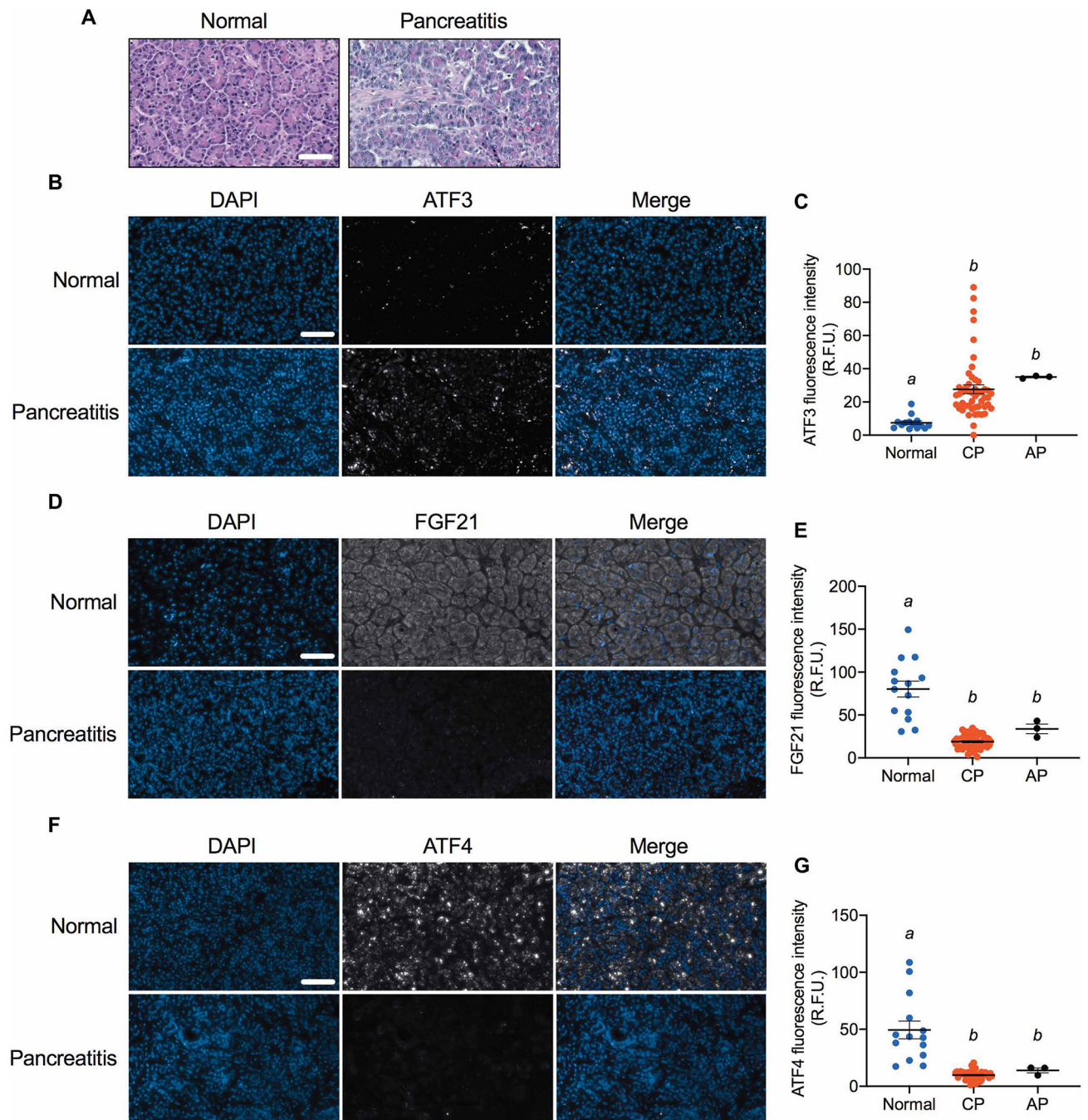


Fig. 5. Pancreatic FGF21, ATF3, and ATF4 concentrations in human patients with pancreatitis. (A) H&E staining of pancreata from a representative normal and pancreatitis patient. (B to G) Pancreatic concentrations of FGF21 (B and C), ATF3 (D and E), and ATF4 (F and G) in normal individuals and patients with chronic (CP) and acute (AP) pancreatitis. Representative immunofluorescence images are shown in (B), (D), and (F), and quantification of samples (normal, $n = 14$; chronic, $n = 49$; and acute pancreatitis, $n = 3$) is shown in (C), (E), and (G). In the immunofluorescence images, DAPI staining is blue and FGF21, ATF3, and ATF4 stainings are gray. Scale bar indicates 50 μm for all images.

Results in (C), (E), and (G) are expressed as means \pm SEM. Statistical differences ($P > 0.05$) are indicated between all values that have different letters. R.F.U., relative fluorescence units.

Author Manuscript

Author Manuscript

Author Manuscript

Author Manuscript

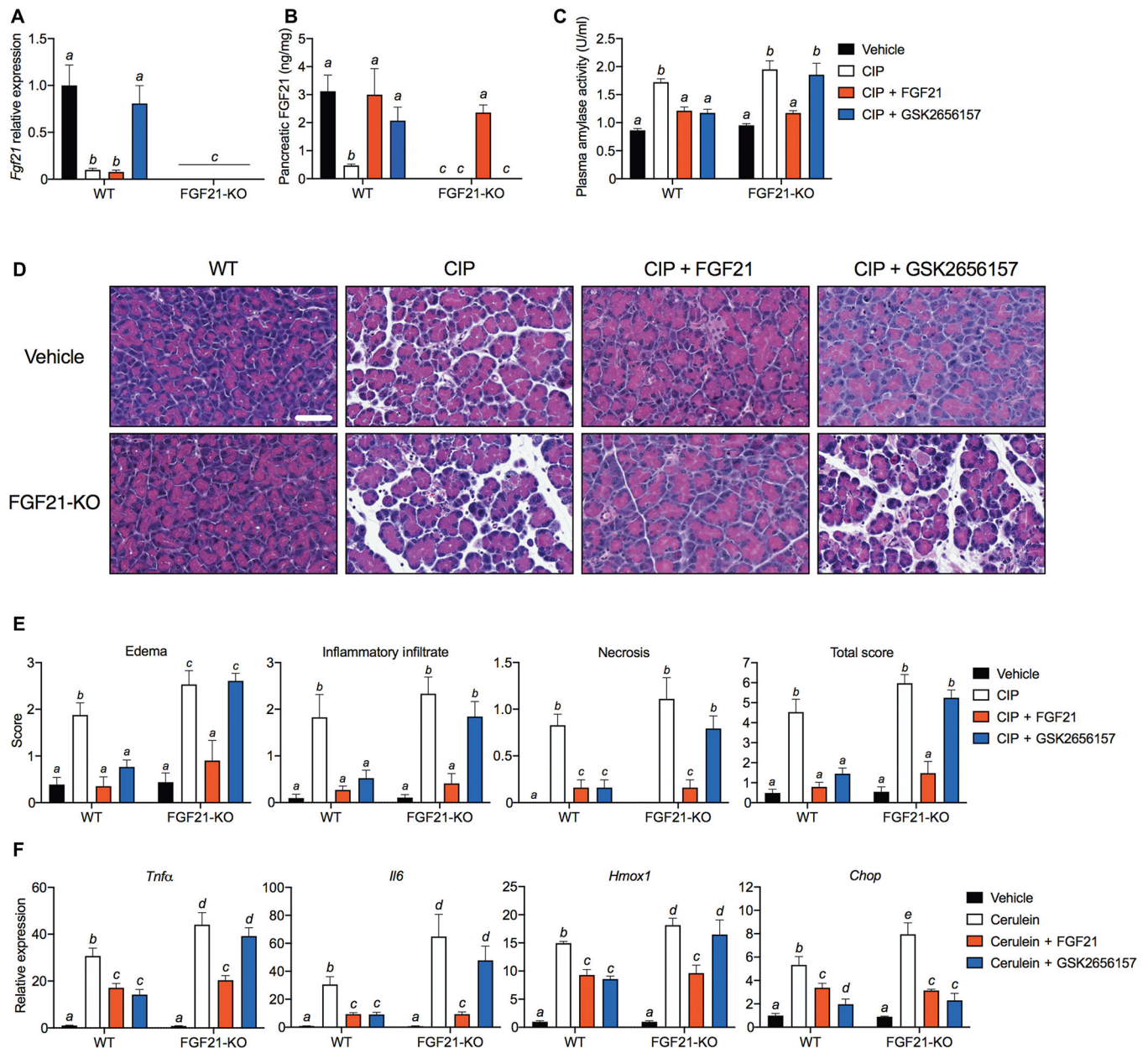


Fig. 6. Inhibition of PERK ameliorates pancreatitis in an FGF21-dependent manner.

(A to F) Wild-type (WT) or FGF21 KO mice (FGF21-KO) were treated with FGF21 (1 mg/kg) or GSK2656157 (25 mg/kg) (four intraperitoneal injections) after CIP. (A and B) Pancreatic FGF21 mRNA (A) and protein (B). (C to F) Plasma amylase activity (C), representative H&E images (D), histological grading (E), and pancreatic mRNA markers of inflammation (*Tnfa* and *Il6*), oxidative stress (*Hmox1*), and ER stress (*Chop*) (F) in mice treated with therapeutic or vehicle control. Scale bar indicates 50 μ m for all images. Results are expressed as means \pm SEM; $n = 6$ mice per group. Statistical differences ($P > 0.05$) are indicated between all values that have different letters.